

Stellar Spiral Structures in Triaxial Dark Matter Haloes

Shaoran Hu¹, Debora Sijacki¹

¹ *Institute of Astronomy and Kavli Institute for Cosmology, University of Cambridge, Madingley Road, Cambridge CB3 0HA*

2 July 2022

ABSTRACT

We employ very high resolution simulations of isolated Milky Way-like galaxies to study the effect of triaxial dark matter haloes on exponential stellar disks. Non-adiabatic halo shape changes can trigger two-armed grand-design spiral structures which extend all the way to the edge of the disk. Their pattern speed coincides with the inner Lindblad resonance indicating that they are kinematic density waves which can persist up to several Gyrs. In dynamically cold disks grand-design spirals are swing amplified and after a few Gyrs can lead to the formation of (multi-armed) transient recurrent spirals. Stellar disks misaligned to the principal planes of the host triaxial halo develop characteristic integral shaped warps, but otherwise exhibit very similar spiral structures as aligned disks. For the grand-design spirals in our simulations their strength dependence with radius is determined by the torque on the disk, suggesting that by studying grand-design spirals without bars it may be possible to set constraints on the tidal field and host dark matter halo shape.

Key words: methods: numerical – galaxies: spiral – galaxies: haloes

1 INTRODUCTION

For many years spiral structures in galaxies have been the subject of extensive observational, theoretical and numerical studies, but their origin still remains unclear. While the morphologies of spiral structures vary considerably, they can be generally classified into two broad categories: “grand-design” spirals with mostly two arms that extend over a large range of radii and “flocculent” spirals that consist of many small fragments of arms. Both kinds of spirals are mostly trailing rather than leading. The Milky Way, for example, is known to have a two-folded grand-design spiral structure and several secondary arms (Churchwell et al. 2009).

The nature of the two kinds of spirals may be different. The “grand-design” spiral structures are often attributed to a perturber, e.g. a strong bar or a nearby object. M51 with its companion NGC 5195 is a well-known example of a grand-design two-folded spiral galaxy with a companion (Arp 1966). Generally, the spiral arms are not “material arms”, in which case the stars would stay in the arms forever and the spiral arms would wind up quickly due to the differential rotation of the disk.

Lindblad proposed a theory of quasi-stationary spiral structures for grand-design spirals (e.g. Lindblad 1963). In his theory, spiral structures are in fact kinematic density waves with a pattern speed of $\Omega_P = \Omega - \kappa/n$ (with n typi-

cally equal to 2). In a frame moving with this pattern speed, the orbits of the epicyclic motion of the stars become ellipses without precession, which guarantees that the density field of the disk remains constant in this rotating frame. When orbits are arranged in a way that the highest density falls into a spiral-like shape (e.g. Kalnajs 1973), constantly rotating stationary grand-design spiral structures can survive in the disk (Lindblad 1956). Lin & Shu (1964) developed a theory of density waves of quasi-stationary spiral structures further. They regarded spiral structures as large-scale waves propagating through the disk in a linear regime (see also Bertin & Lin 1996).

The “flocculent” spiral structures (and some of the “grand-design” spirals) are considered to be caused by instabilities due to self-gravity. To form spiral structures of this kind, two important processes are needed: swing amplification of small perturbations and a feedback loop. The local stability of a disk with respect to axisymmetric perturbations is characterised by Toomre’s Q parameter (Toomre 1964). For stellar disks we have

$$Q = \frac{\sigma_R \kappa}{3.36 G \Sigma}, \quad (1)$$

where σ_R is the velocity dispersion in the radial direction, κ is the epicyclic frequency and Σ is the surface density. When $Q > 1$, the disk is locally stable to axisymmetric instabilities, while for $Q < 1$, the disk becomes locally unstable. Considering the case of non-axisymmetric perturbations, Goldreich & Lynden-Bell (1965) studied the stability of differentially rotating disks and showed that due to self-gravity, small perturbations can be greatly amplified. Toomre (1981) explored

* E-mail: sh759@ast.cam.ac.uk

the theory further into the non-linear regime with the aid of numerical experiments and showed that strong swing amplification can occur when Q is slightly higher than 1, i.e. if the disk is locally stable but the self-gravity is still strong and the wavelength ratio X is appropriate (typically between 1 and 3):

$$X = \frac{k_{\text{crit}}R}{m} = \frac{\kappa^2 R}{2\pi G\Sigma m}, \quad (2)$$

where R is the radius, m is the number of arms and $k_{\text{crit}} = \kappa^2/(2\pi G\Sigma)$ is the critical wavelength of the swing amplification. In this process small leading waves are amplified to strong trailing waves and the amplification factor can be as high as 100. Toomre (1981) also demonstrated that swing amplification can act on global spiral patterns and greatly amplify their strength, though external torques, for example, are sufficient to form those patterns.

To actually form structures in the disk a feedback loop may also be needed. Feedback in density waves can turn amplified trailing waves back into leading waves so that they can be amplified repeatedly. A sharp outer edge, a wave propagating through the centre of the disk and non-linear interactions are all possible ways of generating feedback (Binney 1987).

Due to the non-linear nature of spiral structures, numerical studies are a necessary tool to fully explore their formation and evolution. For flocculent spirals, early studies (e.g. Miller 1972) have found that self-excited transient recurrent spiral structures can develop in N-body simulations of dynamically cool collisionless systems. Nowadays, this phenomenon is generally understood as the swing amplification of the Poisson noise in the disk.

While a number of past numerical studies found that spirals fade out quickly over time (for a recent review see Dobbs & Baba 2014, and references therein), Fujii et al. (2011) showed that in a stellar disk with more than a few million particles spiral arms could persist for longer periods of time, indicating that previous results were suffering from discreteness effects. Similarly, D’Onghia et al. (2013) showed that with a sufficiently high number of particles (of the order of 10^8), stellar disks with Q slightly larger than 1 can stay stable over a few galactic years. When, however, density perturbations are introduced in the disk (in the form of heavy particles), a transient spiral pattern forms which itself can act as the source of newly formed spiral arms. Furthermore, Sellwood (2012) studied the growth of the transient spiral structures over secular timescales. They found that the maximum strength of the transient spiral structures developed in their N-body simulations with an initially axisymmetric setup does not sensitively depend on the number of star particles, but that it takes longer for a simulation with more star particles to reach the maximum spiral strength (see also Fujii et al. 2011). Stars are scattered at the inner Lindblad resonance as the transient spiral structures form, leading to a re-distribution in the action space, which has been recently confirmed by Fouvry & Pichon (2015) who employed an analytic approach. Taken together, these recent numerical works indicate that to study stellar spiral structures, disks need to be represented with a very high number of resolution elements, to both minimise artificial spiral heating and unrealistic swing amplification of poorly resolved disks.

For the triggering mechanism of the grand-design spiral structures, additionally to bars and close companions, torques caused by the host dark matter halo have been invoked as well. Even though the properties of dark matter haloes, such as their exact shape and mass distribution (and the back-reaction of baryons), are still not precisely known, already early simulations (e.g. Barnes & Efstathiou 1987; Frenk et al. 1988) have indicated that the haloes are generally triaxial. Follow-up studies with a variety of configurations, including dispersionless gravitational collapse models (Warren et al. 1992), self-interacting dark matter models (Yoshida et al. 2000), haloes formed in different cosmological models (Jing et al. 1995; Thomas et al. 1998), and more recent higher resolution studies (e.g. Bryan et al. 2013; Zhu et al. 2015) all find that the dark matter haloes are triaxial. Several generalisations of analytical, spherical halo models that include halo triaxiality were also proposed (Jing & Suto 2002; Bowden et al. 2013). It is generally believed that the inclusion of baryons leads to a reduction of halo triaxiality (Dubinski 1994; Zemp et al. 2012; D’Onghia et al. 2010; Bryan et al. 2013; Zhu et al. 2015), with haloes becoming more oblate, especially in the central region. However, the resulting mildly triaxial halo mass distribution may still impart a significant torque onto the disk of the central galaxy.

In fact, DeBuhr et al. (2012) have found that the gravitational potential of a disk can flatten the halo, while in return bars and warps can develop in the disk under the influence of the flattened halo. For grand-design spiral structures, Dubinski & Chakrabarty (2009) studied the impact of external torque on the disk. In their simulations it is assumed that while the inner part of the dark matter halo is aligned with the disk, the outer region is misaligned and tumbling, causing an external torque. Under such external torque, Dubinski & Chakrabarty (2009) found that grand-design two-folded spiral structures can develop in the disk, along with warps and bars. More recently, Khoperskov et al. (2013) found that grand-design spiral patterns can form in disks within haloes which are gradually turned from spherical into triaxial (see also Khoperskov & Bertin 2015).

None the less, the relation between the triaxiality of dark matter haloes and the spiral structures in disks is still not fully understood. Therefore, a careful study employing very high resolution disks is needed to understand the influence of halo shapes on the disk structure which is the aim of this paper. Also since there are two different kinds of spiral structures, grand-design and flocculent ones, it is important to understand how they form in triaxial haloes.

The paper is organised as follows. In Section 2 we introduce the methodology and the model we use. Our results are then presented in Section 3. In Section 3.1 we examine the numerical effects caused by the finite resolution of simulations which act as perturbations of the density field of stellar disks. In Section 3.2 we study the effect of how triaxial haloes are introduced into the system with very high resolution simulations. Then we focus on the impact of triaxial haloes of different shapes on the disks in Section 3.3. In Section 3.4 we discuss the nature of transient spirals that emerge out of grand-design spiral structures due to non-linear effects. In Section 3.5 we investigate simulations with disks misaligned with the major axes of the halo. Finally, in Section 4 we summarise our results.

2 METHOD

2.1 The Numerical Approach

We perform simulations of stellar disks embedded in different dark matter halo models with GADGET-3, whose previous version GADGET-2 is described in (Springel 2005). GADGET-3 is a N-body/SPH code. In the code, stars are represented by a finite number of stellar particles. Our choice of the number of star particles varies from 10^5 to 10^8 , so for a Milky Way-like galaxy a single star particle in the simulation typically represents about 10^6 to 10^3 stars. Star particles together form a collisionless system, which is simulated with the N-body algorithm.

Gaseous component is very important in the evolution of galactic disks. By interacting with the stars through gravity, gas can enhance the self-gravity of the disk. Also it can develop sharp shocks when placed in a gravitational potential caused by spiral structures (Gittins & Clarke 2004; Dobbs & Bonnell 2006, 2007). Moreover, new stars formed out of the high density gas clumps can act as a cooling source to the dynamical temperature of the disk by lowering the velocity dispersion. However, modelling gas numerically is very difficult, given that complex cooling and heating processes need to be taken into account. Therefore we do not include gaseous component in this work.

Analytic representation of dark matter haloes are employed in all of the simulations. Given that the total mass of the dark matter halo is much larger than the total mass of the disk, if we represent dark matter halo with particles, we need much more dark matter halo particles than star particles (a number that turns out to be prohibitively large!), so that the Poisson noise in the halo is comparable to that in the disk. In fact, for testing purposes, we ran a simulation of a live disk within a live halo, both of them with 10^8 particles. In this simulation, strong transient spiral structures form almost instantly, making it impossible to study the possible effects of the halo shape on the disk. To avoid this effect we would need much more dark matter particles. However, we are primarily interested in the behaviour of the disk rather than that of the dark matter halo. To make sure that the halo does not induce numerical artifacts to the system and to direct computational resources on the object we are interested in, we used analytic dark matter halo models rather than the dark matter particles. It is worth mentioning that with our methodology we cannot study the back-reaction of the disk onto the dark matter halo. To somewhat mitigate this issue, we study static dark matter haloes of different shapes.

For computation of the gravity, the GADGET-3 code employs the TreePM method (Springel 2005). The combination of the two methods, the Tree method and the Particle-Mesh (PM) method, gives us high efficiency in calculating gravitational forces with high accuracy. Constant gravitational softening length ϵ_{grav} for star particles is used in all simulations. Typical values of ϵ_{grav} used in our simulations are shown in Table 1.

2.2 Modelling of Stellar Disks

We set up our disk model following the description in Springel et al. (2005). The disk has an exponential surface

Table 1. Numerical parameters for simulations with different number of star particles. For simulations listed below, the total mass of the stars is either $M_* = 1.9 \times 10^{10} M_\odot$ ($Q \sim 1$ disks) or $M_* = 9.5 \times 10^9 M_\odot$ ($Q > 1.3$ disks). Number of star particles N , mass of a single star particle, m , and gravitational softening length, ϵ_{grav} , are listed below.

$M_* [M_\odot]$	N	$m [M_\odot]$	$\epsilon_{\text{grav}} [\text{pc}]$
1.9×10^{10}	10^5	1.9×10^5	163
1.9×10^{10}	10^6	1.9×10^4	76
1.9×10^{10}	10^7	1.9×10^3	35
1.9×10^{10}	10^8	1.9×10^2	16
9.5×10^9	10^5	9.5×10^4	163
9.5×10^9	10^6	9.5×10^3	76
9.5×10^9	10^7	9.5×10^2	35
9.5×10^9	10^8	95	16

density profile and an isothermal sheet profile vertically, described by

$$\rho_*(R, z) = \frac{M_*}{4\pi z_0 R_S^2} \text{sech}^2\left(\frac{z}{z_0}\right) \exp\left(-\frac{R}{R_S}\right), \quad (3)$$

where $R_S = 3.13 \text{ kpc}$ is the scale length of the disk, M_* is the total mass of the stars and $z_0 = 0.1 R_S$ is the scale height. The total mass of the system, $M_T = M_* + M_{\text{dm}}$ is $9.5 \times 10^{11} M_\odot$ in all our simulations. However, two kinds of disks with different disk mass ratios $m_d = M_*/M_T$ are used: one with $m_d = 0.02$ and minimum Toomre's Q parameter $Q_{\text{min}} \sim 1$, the other with $m_d = 0.01$ and $Q > 1.3$. The radial profiles of Q parameter for different disks and as a function of time are shown in Figure A2 in the Appendix. The circular velocity and velocity dispersion of the stars in the disk are worked out analytically based on the density distribution of the system.

2.3 Spherical Dark Matter Haloes

Both Hernquist (Hernquist 1990) and triaxial dark matter haloes derived from it are used as our halo models. The Hernquist profile of a halo is described by

$$\rho_{\text{HQ}}(r) = \frac{M_{\text{dm}}}{2\pi} \frac{a}{r(r+a)^3}, \quad (4)$$

where $a = 30 \text{ kpc}$ is a scale length factor that controls the distribution of the mass. The potential of the Hernquist halo is given by

$$\Phi_{\text{HQ}}(r) = -\frac{GM_{\text{dm}}}{r+a}. \quad (5)$$

Here, the mass of the halo is $M_{\text{dm}} = M_T(1 - m_d)$. The virial radius of the halo, R_{200} , is set to be 160 kpc.

2.4 Triaxial Dark Matter Haloes

To derive a triaxial halo from a Hernquist halo, we followed Bowden et al. (2013) and added two low-order spherical harmonic terms to the potential, i.e.

$$\Phi(r, \theta, \phi) = \Phi_{\text{HQ}}(r, \theta, \phi) + \Phi_T(r, \theta, \phi), \quad (6)$$

with the triaxial part $\Phi_T(r, \theta, \phi)$ being

$$\Phi_T(r, \theta, \phi) = 4\pi G \frac{\rho_1 r_1^4 r}{(r+r_1)^3} Y_2^0(\theta, \phi) - 4\pi G \frac{\rho_2 r_2^4 r}{(r+r_2)^3} Y_2^2(\theta, \phi),$$

Table 2. Halo models used in this work. a , b and c are major axis lengths of iso-density surface in x , y and z direction. p and q are the ratios of b to a and c to a . The suffixes of the two parameters, 0 and ∞ , indicate whether the parameter is for the inner or the outer limit. In model T_{O1} and T_{O2} , the disks do not lie in the $x - y$ plane. The position of the disk plane is decided by 1) setting coordinates $x' - y' - z'$ to initially coincide with $x - y - z$ coordinates, 2) rotating $x' - y' - z'$ coordinates along the z' axis for an angle α , 3) rotating $x' - y' - z'$ coordinates along the x' axis for an angle β and 4) putting the disk in the $x' - y'$ plane.

Model	p_0	q_0	p_∞	q_∞	α	β
S	1	1	1	1	0	0
T_1	0.6	0.4	1	1	0	0
T_2	0.95	0.85	0.6	0.5	0	0
T_3	0.85	0.85	0.85	0.85	0	0
T_{O2}	0.95	0.85	0.6	0.5	0	$\pi/4$

(7)

where Φ_{HQ} is the potential of the Hernquist profile and $Y_2^0(\theta, \phi) = \frac{3}{2} \cos^2 \theta - \frac{1}{2}$, $Y_2^2(\theta, \phi) = 3 \sin^2 \theta \cos 2\phi$ are spherical harmonic functions.

Hence,

$$\rho(r, \theta, \phi) = \rho_{\text{HQ}}(r, \theta, \phi) - 4\rho_1 \frac{r_1^4(r_1^2 + 5r_1r + r^2)}{(r + r_1)^5 r} Y_2^0(\theta, \phi) + 4\rho_2 \frac{r_2^4(r_2^2 + 5r_2r + r^2)}{(r + r_2)^5 r} Y_2^2(\theta, \phi). \quad (8)$$

Here ρ_1 , r_1 , ρ_2 and r_2 are four free parameters that can be used to control the shape of the halo in the inner and outer regions, i.e. the ratio of major axis lengths of the iso-density surface in y and x direction at the inner and outer limit, $p_0 = \lim_{r \rightarrow 0} b/a$ and $p_\infty = \lim_{r \rightarrow \infty} b/a$ and similarly in z and x direction, $q_0 = \lim_{r \rightarrow 0} c/a$ and $q_\infty = \lim_{r \rightarrow \infty} c/a$. For most of the simulations the disk lies in the $x - y$ plane, but we also ran several simulations in which the disks have a 45° angle to the $x - y$ plane.

The names and parameters of all halo models are listed in Table 2. The S model is the original spherical Hernquist halo. T_1 model is spherical outside and triaxial inside, while T_2 is the opposite. In T_3 model, the inner and outer limit of the major axis length ratios are $p_0 = q_0 = p_\infty = q_\infty = 0.85$. However the major axis length ratios p and q are not constant throughout the halo. As shown in Figure 7, the ratio p is slightly lower than 0.85 for $0 < R < 5R_s$. This is due to the fact that we are using an analytical model for the triaxial halo, which only constrains the ratios of major axis lengths for the $r \rightarrow 0$ and the $r \rightarrow \infty$ limits. The parameters for T_2 are chosen to be comparable to the results of cosmological simulations described in Zemp et al. (2012).

3 RESULTS

3.1 Finite Resolution Effects

We start by first investigating the finite resolution effects on the disk properties by using an increasing number of star particles to represent the disk. In total we ran five simulations with the same S halo, i.e. spherical Hernquist halo

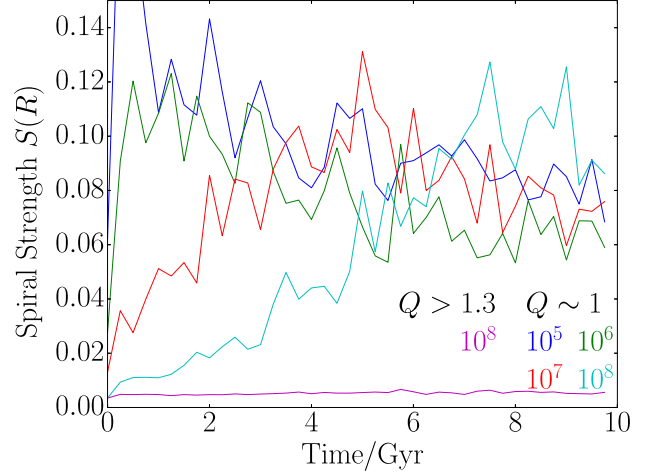


Figure 1. The growth of transient spiral structures with time for disks with 10^5 , 10^6 , 10^7 and 10^8 particles. Spiral strength $S(R)$ is defined in equations (9) and (10), where all $m \leq 12$ modes are taken into account. Spiral structures grow in all four $Q \sim 1$ disks, but not in the $Q > 1.3$ disk. The scale time for growing spirals is longer for simulations with more star particles. For simulation with 10^5 to 10^7 star particles, spiral strength decreases after reaching the peak value due to the spiral heating.

without any triaxial terms, but with different disk mass ratio m_d and different numbers of star particles in the disk. For one of these simulations, we used a $m_d = 0.01$ disk with 10^8 star particles. As mentioned before, in this disk model, Toomre's Q parameter is greater than 1.3 throughout the disk. For the rest of the simulations, m_d is set to 0.02 and we use from 10^5 to 10^8 star particles. For some regions in these disks, $Q \sim 1$, which means that they are unstable to swing amplification.

In simulations with $Q \sim 1$ disks, transient spiral structures develop. As shown in Figure A1 in Appendix A, these spiral structures are multi-armed, typically from 7-armed to 10-armed. The strength of these spiral structures at radius R can be quantified with

$$S(R) = \sqrt{\sum_{m=1}^{12} \left| \frac{\hat{\Sigma}_m(R)}{\hat{\Sigma}_0(R)} \right|^2}, \quad (9)$$

where $\hat{\Sigma}_m(R)$ is the Fourier transformation of the surface density $\Sigma(R, \theta)$ of the disk at fixed radius R along the azimuthal coordinate θ , i.e.

$$\hat{\Sigma}_m(R) = \frac{1}{2\pi} \int_{-\pi}^{\pi} \Sigma(R, \theta) e^{-im\theta} d\theta. \quad (10)$$

Here we sum over $m = 1$ to 12 to include the effect of all spiral structures with $m \leq 12$. Structures with higher m , which represent smaller structures in the disk, are excluded because they are subject to random noise in the disk. The evolution of $S(R)$ over a time span of 10 Gyr at a fixed radius $R = 2R_s$ is shown in Figure 1.

Strong spiral structures develop in all four simulations with $Q \sim 1$ disks. The maximum spiral strength for these simulations is roughly the same regardless of the number of star particles. However, simulations with a higher number of particles take longer time to grow spiral structures. This is in agreement with the findings from Sellwood (2012) and

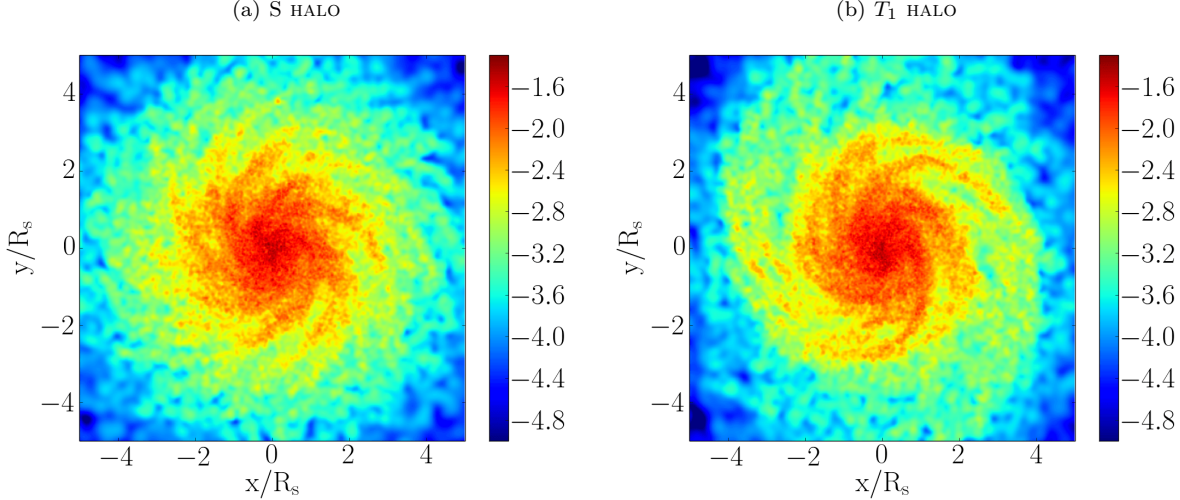


Figure 2. Surface density of a disk in the spherical and the T_1 triaxial halo at time 0.5Gyr. Values on the colour bar are $\log(\Sigma/10^{10}M_{\odot}\text{kpc}^{-2})$, where Σ is the surface density. In both simulations the disk has 10^5 particles. The surface densities of the two disks are similar. This indicates that when the Poisson noise is significant, swing amplification is the dominating factor over the influence of a triaxial halo.

Fujii et al. (2011). In particular, it takes more than 7Gyr for the simulation with 10^8 star particles to fully develop spiral structures. Also note that spiral strength in simulations with 10^5 to 10^7 particles decreases after reaching the maximum, because of spiral heating. For the “dynamically hot” disk with $Q \sim 1.3$, the spiral strength is always low, indicating that the swing amplification is weak, as expected.

To further study the resolution effects, we replace the spherical halo with triaxial haloes described in Table 2. Figure 2 shows the surface density of a 10^5 particle disk in the T_1 halo at time $t = 0.5$ Gyr. T_1 halo is triaxial inside and spherical outside, which means that the non-axisymmetric force introduced by this halo in the central region of the disk is very high. However, the disk in the T_1 halo still develops a multi-armed transient spiral structure, though the distribution the spiral arms is more asymmetric than the one in the spherical halo. This indicates that when the Poisson noise in the disk is very high, swing amplification of the disk dominates the whole process and external torques cannot significantly influence the strength of the arms. To study carefully the effects of triaxial haloes, swing amplification of Poisson noise caused by finite resolution needs to be suppressed. For the rest of this paper, we thus perform simulations with 10^8 star particles, so that the growth of transient spiral structures caused by swing amplification of the Poisson noise in the initial conditions is sufficiently slow.

3.2 Time-dependent Triaxial Haloes

The top row of Figure 3 shows the surface density, density variation with respect to the initial conditions and the residual density of the $Q > 1.3$ disk with 10^8 star particles in the T_2 halo at 3Gyr. Here residual density refers to the normalised density difference to the average surface density over azimuthal coordinate,

$$\Sigma_{\text{res}}(R, \phi) = \frac{\Sigma(R, \phi) - \bar{\Sigma}(R)}{\bar{\Sigma}(R)}, \quad (11)$$

where $\bar{\Sigma}(R)$ is the average density at radius R , i.e. $\bar{\Sigma}(R) = \frac{1}{2\pi} \int_0^{2\pi} \Sigma(R, \phi) d\phi$. We use a $Q > 1.3$ disk to avoid the possible interference due to the swing amplification of the disk, which we study later on in Section 3.4. As shown in the top row of Figure 3 strong grand-design two-armed spiral structures form. These spiral structures are very sharp, tightly wound up and global. Unlike the spiral structures formed due to swing amplification (see Figure A1), which only exist in the intermediate part of the disk (i.e. for $1 \lesssim R/R_s \lesssim 3.5$), the spiral structures in triaxial halo extend to the edge of the disk. This agrees with Dubinski & Chakrabarty (2009) where an external torque due to the tumbling dark matter halo drives the formation of the spiral structures. However, it is unclear whether these spiral structures are caused by the triaxial halo alone or by the impulsive process of introducing triaxial haloes to the system with a disk that is initially in equilibrium with a spherical halo.

To fully understand the formation mechanism of these grand-design spiral structures, we run simulations in which the shape of the halo changes from spherical to triaxial gradually, so that initially the disk is in the equilibrium with the halo and no impulsive change to the system occurs. As shown in equations (6) and (7), the analytic potential we employed in our simulations consists of two parts: a spherical Hernquist potential and a triaxial part. We hereby extend equation (6) so that the triaxial part of the halo can be turned on and off gradually with a function $f(t)$,

$$\Phi(r, \theta, \phi) = \Phi_{\text{HQ}}(r, \theta, \phi) + f(t)\Phi_{\text{T}}(r, \theta, \phi). \quad (12)$$

When $f(t) = 0$, the dark matter halo is a purely spherical Hernquist halo, while when $f(t) = 1$, the dark matter halo is a fully developed triaxial halo.

The bottom row of Figure 3 shows the surface density and the residual density of a simulation with a gradually introduced T_2 halo. In this simulation the growth of the triaxial part of the potential is set to

$$f(t) = 1 - \exp(-t/\tau_1), \quad (13)$$

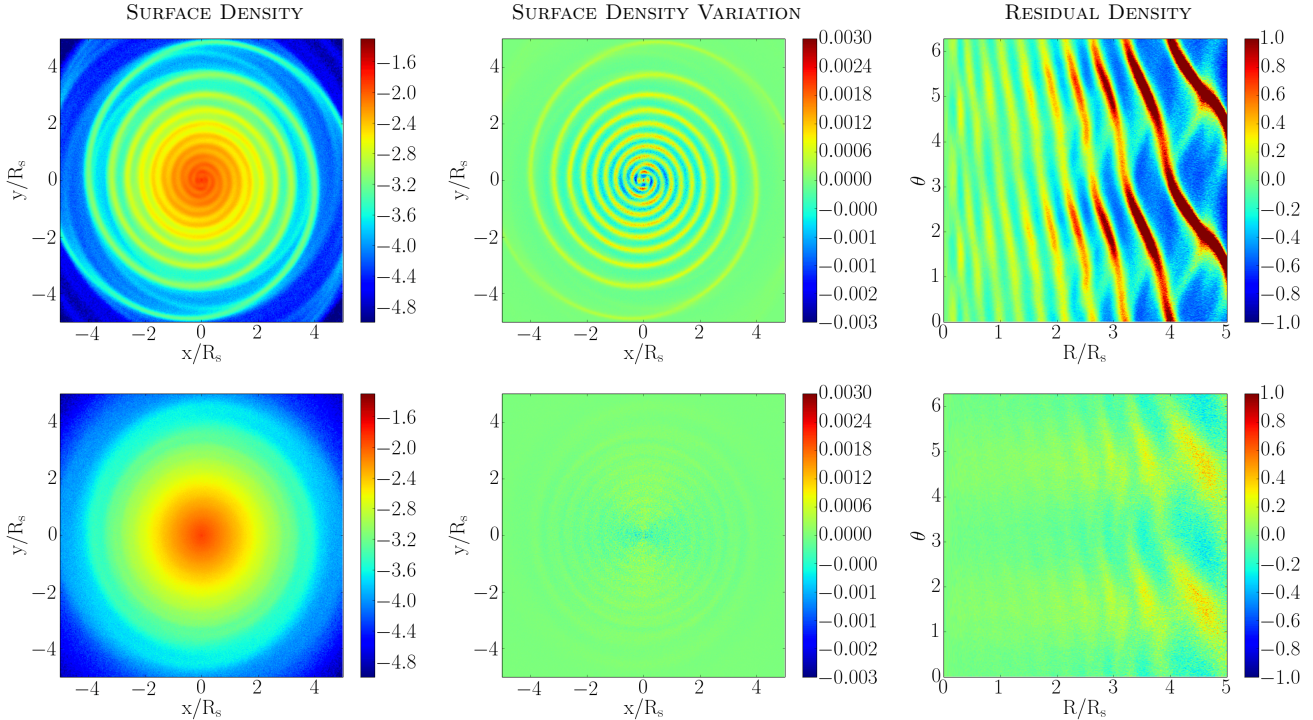


Figure 3. Surface density, i.e. $\log(\Sigma/10^{10}M_{\odot}\text{kpc}^{-2})$, its variation to the initial conditions, and residual density of $Q > 1.3$ disks in a simulations with 10^8 star particles in a T_2 halo at $t = 3\text{Gyr}$. Top row: simulation with a static T_2 halo. Bottom row: halo is initially spherical and then gradually turns into T_2 halo with a scale time of $\tau = 1\text{Gyr}$. In the simulation with a static T_2 halo, strong two-armed spiral structures form. The spiral structures keep winding up after their formation. By the time $t = 3\text{Gyr}$, spirals are tightly wound up. With triaxiality of the halo introduced gradually, very weak spiral structures form in the disk, indicating that the spiral structures found in the simulation with a static triaxial halo are caused by the sudden change of the halo shape.

where the scale time $\tau_1 = 1\text{Gyr}$. The time shown in Figure 3 is 3Gyr , when the triaxial transformation of the halo is almost complete, with $f = 0.95$. With the initially spherical halo growing slowly to triaxial, as shown in the residual density map in the rightmost panel, the spiral structure is very weak inside $3R_s$, while relatively weak two-armed structures develop in the outer region.

The fact that only weak spiral structures develop when the triaxiality of the halo is introduced gradually indicates that triaxial halo alone does not necessarily lead to spiral structures. In fact, by comparing the orbital period τ_O of the stars and the time scale τ_1 of introducing the halo, we find that the time scales of the two processes determine whether a strong spiral structure will develop. The orbital period τ_O is very small in the innermost regions of the disk. The introduction of triaxiality has a much longer time scale $\tau_1 = 1\text{Gyr}$, which can be seen as an adiabatic perturbation in the centre. τ_O becomes longer at larger radii. At $R = 3R_s$, $\tau_O = 0.31\text{Gyr}$, which is still shorter than the τ_1 , but the introduction of the halo is starting to make an effect. At about $R = 5R_s$, $\tau_O \sim 0.5\text{Gyr}$. Now introduction of the triaxial halo can no longer be considered as adiabatic, and the change of halo shape starts to have a significant effect on the disk.

The spiral structures formed in this simulation on larger scales are shown in the first row of Figure 4. Here the normalised density difference to the initial density

$$\overline{\Delta\Sigma} = \frac{\Sigma - \Sigma|_{t=0}}{\Sigma|_{t=0}} \quad (14)$$

is shown so that the structures in outer regions where density is significantly lower can be clearly seen. As shown in different columns (which are for $t = 1, 2$ and 3Gyr), structures form at larger radii and grow inward. However, due to the changing of the halo potential, ring structures also form in the disk and to a certain extent interfere with the spiral structures, making it hard to distinguish genuine spiral structures from rings. We therefore run another simulation with self-gravity in the disk turned off, as shown in the middle row of Figure 4. Two-armed grand-design spiral structures still form in this simulation, but rings do not interfere with spirals through self-gravity anymore. Instead, they superimpose with each other so that the rings are now seen as fine lines in each arm of the spiral structures. We therefore conclude that rings, though forming easily as a response to the change of the halo potential and modifying the shape of the spiral structures, are not essential for the spiral forming process.

We explore this problem further with a smoother $f(t)$ function. We generalised equation (13) to

$$f_i(t) = \left(1 - \frac{1}{i}e^{-t/\tau_1}(1 + (i-1)e^{-t/\tau_1})\right)^i, \quad (15)$$

where i is the smoothing factor and $f_1(t)$ falls to the original form used in equation (13). This generalisation satisfies $f_i(0) = 0$ and $f_i(t) = f_1(t)$ to the first order in e^{-t/τ_1} as $t \rightarrow \infty$. As shown in Figure 5, for a higher i , the growth of $f(t)$ at the early stage of the simulation is smoother. In practice we ran a simulation with $i = 6$. Self-gravity is in-

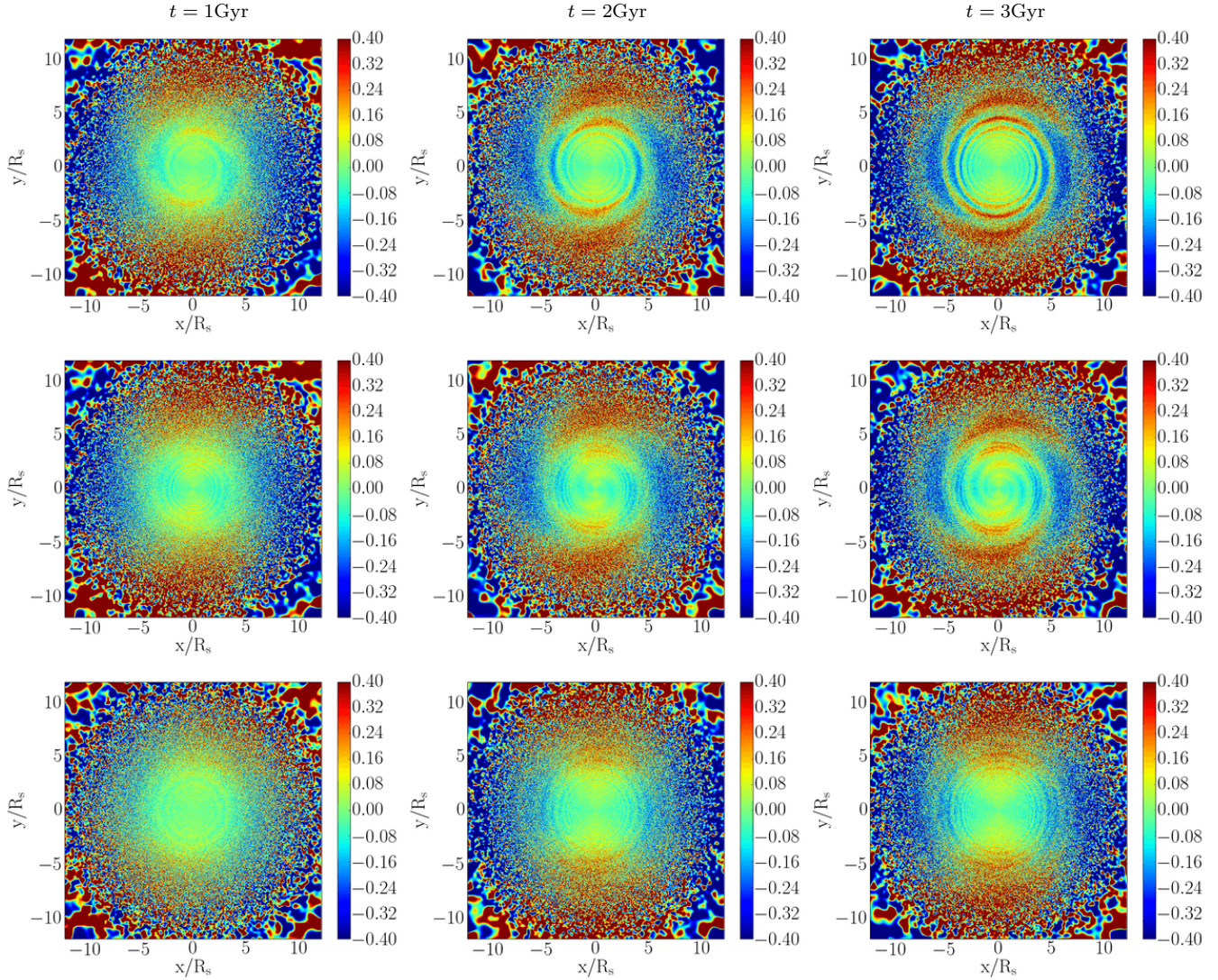


Figure 4. Disks in a T_2 halo with a gradually increasing triaxiality with time. The relative difference of surface density to the initial conditions is shown. Top: with self-gravity. Middle: without self-gravity. Bottom: with self-gravity and a smoother introduction of triaxiality in the halo, i.e. $f_6(t)$ as defined in equation (15). With self-gravity in the disk turned off, it can be clearly seen that a two-armed spiral structure forms outside and grows inward. However for the simulation with self-gravity, this spiral pattern interferes with rings that form due to the change of halo profile. When the triaxiality of the halo is introduced in a smoother way, no prominent spiral structures can be found. This indicates that disks can survive in triaxial haloes without developing spiral structures if the shape of the halo changes smoothly enough.

cluded in this simulation as well. The result of this simulation is shown in the bottom row of Figure 4. No prominent spiral structures develop. This demonstrates that the triaxial shape of a halo itself does not necessarily lead to spiral structures. Rather, non-adiabatic change of the halo shape, i.e. halo changing on a time scale shorter or comparable to the orbital period of the stars, will cause grand-design spiral structures to form.

Khoperskov et al. (2013) has reported that in their simulations similar grand-design two-armed spiral structures form within a halo growing slowly enough from a spherical one to a triaxial one with a time scale more than four times longer than the rotation periods of the stars at the outer part of the disk. In contrast, we have shown in Figure 4 that with a carefully chosen growth function $f(t)$ of

the triaxiality of the halo, the development of the spiral patterns is not necessary. We therefore conclude that the spiral structures formed in their simulations are also due to the fact that the introduction of the triaxiality is not adiabatic enough.

To understand if triaxial haloes are needed for these grand-design spiral structures to survive for longer periods of time, we also run a simulation with the halo shape turning from triaxial to spherical abruptly, with

$$f(t) = \exp(-(t/\tau_D)^2), \quad (16)$$

with a time scale $\tau_D = 0.2\text{Gyr}$. In this simulation strong spiral structures form at the beginning of the simulation almost instantly, as expected. We run simulation further in time and find that the spiral structures can persist for much longer time. The surface density, its variation to the initial

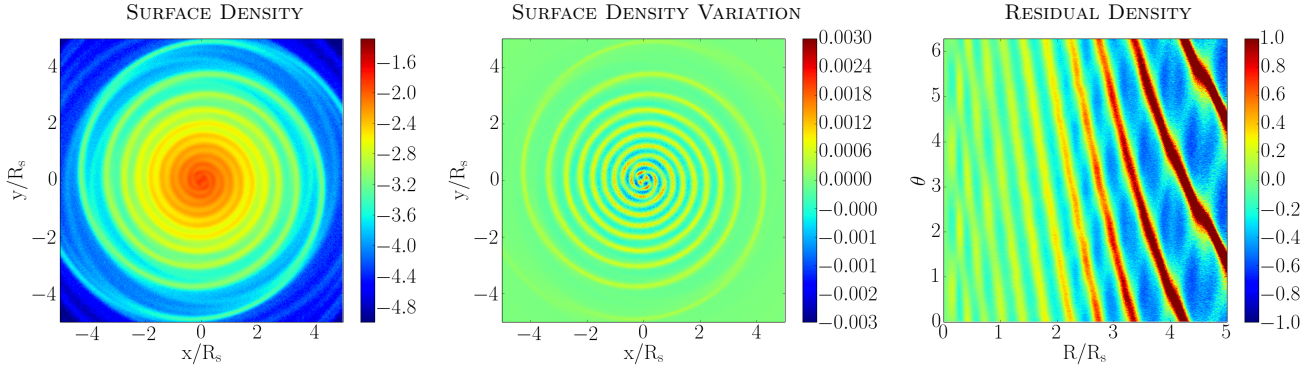


Figure 6. Simulated disks at $t = 3$ Gyr in a halo that has a time-dependent triaxiality. Halo starts as the T_2 halo, but is quickly turned into a spherical halo with a scale time of $\tau = 0.2$ Gyr. The grand-design spiral structures still exist for a long time, indicating that once formed, grand-design spiral patterns can survive in a spherical halo.

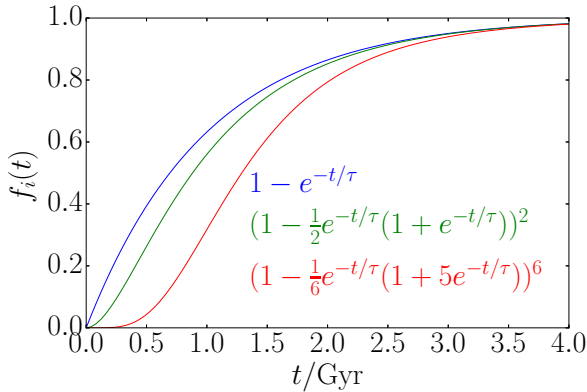


Figure 5. Time dependence of $f_i(t)$ for smoothing factor $i = 1, 2$ and 6 . $f_i(t)$ shows the same trend as $f_0(t)$ as $t \rightarrow \infty$. However higher i indicates a smoother growth of f_i at the beginning of the simulation.

conditions and the residual density of the disk at $t = 3$ Gyr is shown in Figure 6. At 3 Gyr, $f = 1.9 \times 10^{-98}$, meaning that the halo is extremely close to being spherical. In fact, the halo is already extremely close to spherical as early as $t = 1$ Gyr, with $f(t) = 1.4 \times 10^{-11}$. Spiral structures survive in this spherical halo for at least 2 Gyr and remain strong. Therefore, triaxial haloes, proven above not necessary for forming spiral structures, are not needed for persisting spiral structures either.

It is interesting to note that Toomre (1981) studied properties of a disk galaxy with an external torque turned on and off rapidly. Though both in Toomre’s and in our simulations, two-armed spiral structures form, they are different in at least two ways. First, in Toomre (1981), the Toomre’s Q parameter and the wavelength ratio X are both in the range that favours the swing amplification of $m = 2$ modes, while in our simulation, for $m = 2$ the wavelength ratio X is too high for swing amplification to become significant. Actually in our simulations the modes for the X to fall into the range $1 < X < 3$ that favours the swing amplification require $7 \lesssim m \lesssim 10$, which are the typical number of arms for transient spiral structures seen in Fig-

ure A1. Therefore, though the swing amplification plays an important role in the development of the grand-design spiral structures in Toomre (1981), it plays a minor role in our simulations. In fact, as shown later in Section 3.4, the swing amplification may destroy the grand-design spiral structures at later times. Second, Toomre (1981) found that the grand-design spiral structures in their simulation decay after several rotational periods, while in our simulations the grand-design spiral structures can survive for a longer time. While disk properties and simulation methodology in our work is quite different, this indicates that the formation mechanism of the spiral structures may be different in Toomre (1981) and our simulations. In fact, the spiral structures in our simulations can be well explained by the kinematic density wave theory, as shown in Section 3.4.

3.3 Dependence of Spiral Strength on the Halo Shape

We performed three additional simulations to further study the influence of different halo shapes on the spiral structure strength. In these simulations, we employ disks with $Q \sim 1$ and various static triaxial dark matter haloes. The disk is originally in equilibrium with a spherical halo. An abrupt introduction of the triaxiality in the halo, is the cause of spiral structures, as shown in Section 3.2.

Three halo models, T_1 , T_2 and T_3 , introduced in Table 2, are used in these simulations. The ratio of major axes, $p = b/a$, of these haloes at different radii is shown in the left panel of Figure 7. T_1 model is more triaxial inside, T_2 model is more triaxial outside, and the ratio of the major axis of the halo in the T_3 model is equal at the innermost and the outermost limits, and slightly lower in between. In all three simulations, spiral structures develop instantly in response to the abrupt change of the halo shape from the spherical one. Surface density Σ , residual density Σ_{res} and the relative spiral strength of different m modes, S_m , of the disks in these simulations are shown in Figure 8. Here the relative spiral strength S_m is defined as

$$S_m(R) = \left| \frac{\hat{\Sigma}_m(R)}{\hat{\Sigma}_0(R)} \right|, \quad (17)$$

where $\hat{\Sigma}_m(R)$ is the Fourier transformation of the surface density of the disk at radius R along the azimuthal coord-

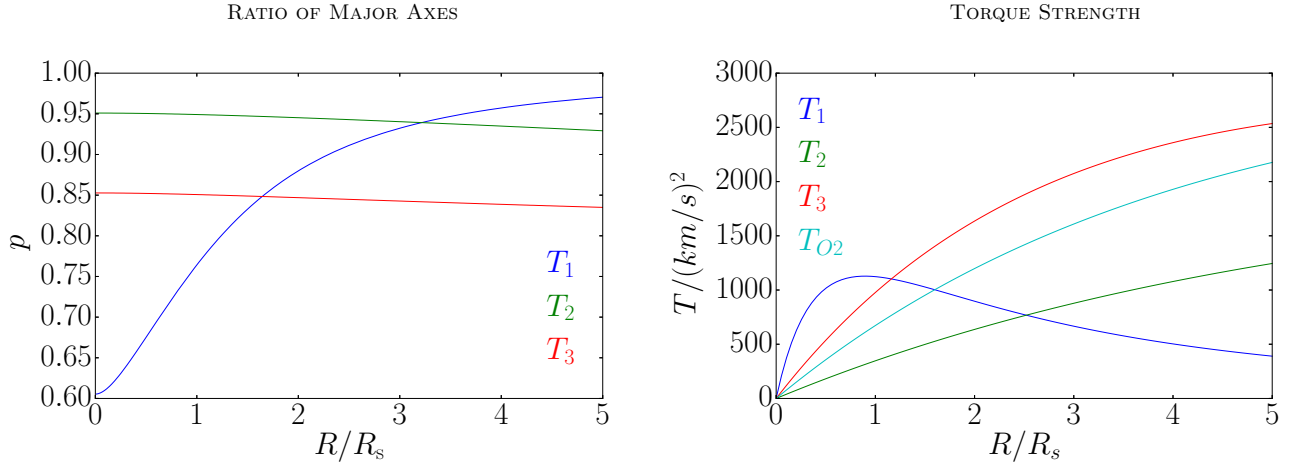


Figure 7. Shape and torque strength of the dark matter halo models as a function of R/R_S . Left: ratio of major axes, $p = b/a$, as a function of R/R_S for halo models T_1 , T_2 and T_3 listed in Table 2. Right: absolute value of the torque perpendicular to the disk plane that a star with azimuthal coordinate $\theta = \pi/4$ and radius R feels for simulations with halo models T_1 , T_2 , T_3 and T_{O2} . The simulation with halo model T_{O2} is discussed later in Section 3.5.

ordinate, as defined in equation (10). In practice, the spiral strength fluctuates over time at a given radius. To show the mean trend of the strength with respect to the radius, we therefore plot the averaged spiral strength over a time interval from 0.35 Gyr to 0.85 Gyr.

As shown in the top three rows of Figure 8, two-armed spiral structures form in all three simulations. The spiral strength for $m = 2, 4, 6$ and 8 has a similar radial profile within each simulation, indicating that the spiral strength measured for higher m modes is largely due to the two-armed spiral structures. However for different simulations, the relative spiral strength, S_m , varies differently with radius R . Generally, spiral strength depends on the halo triaxiality. This can be understood by comparing the torque generated by the triaxial halo, as shown in the right panel of Figure 7. The torque and the strength of the spiral structures show almost identical trends as a function of radius for all three simulations, i.e. by comparing different simulations, one can find that the strength of the spiral structures at a given radius is stronger for the simulation where the torque at that radius is stronger, and vice versa.

3.4 Swing Amplification of Spiral Fragments

As shown in Figure 1, for a $Q \sim 1$ disk with 10^8 star particles located in a spherical halo, transient spiral structures develop in several Gyrs due to swing amplification. To explore if this process will also take place in simulations with a triaxial halo, we run the simulation with a T_2 halo for a longer time.

As shown previously in Figure 8, at first only two-armed spiral structures develop in the disk. However after some time transient multi-armed spiral structures gradually form in the central region of the disk. Various properties of the disk in this simulation at $t = 3$ Gyr are shown in Figure 9. It can be seen from the surface density of the disk that two kinds of spiral structures co-exist in the disk, with transient spiral arm structures dominating the inner region of the disk,

and two-armed grand-design spiral structures taking up the outer region.

For regions where $Q < 1$, the disk is unstable to axisymmetric perturbations, and for regions where Q is slightly higher than 1, the disk is unstable to the swing amplification. Figure 9 shows that regions with $Q < 1$ lie perfectly within the spiral structures. This indicates that the spiral arms, with their higher density, can attract more stars into the spiral arms, hence magnifying the strength of the spiral structures. Also, in the part of the disk with $R_S < R < 3.5R_S$, the Q parameter is generally slightly higher than 1 outside of the spiral structures. This explains why transient spiral structures form in this region due to swing amplification, while for $R > 3.5R_S$ azimuthally averaged Q value is significantly higher than 1.

To further explore the interaction between grand-design spiral structures and swing amplification, we compare the disks formed in three different simulations: one with a $Q \sim 1$ disk in a T_2 halo, one with a $Q \sim 1$ disk in a spherical halo, and one with a $Q > 1.3$ disk in a T_2 halo. The surface density and residual density of the disks in these simulations at $t = 3$ Gyr are shown in Figure 10. By comparing the simulations with $Q \sim 1$ and $Q > 1.3$ disk in T_2 haloes, one can see that the transient arms do not form in the simulation with the $Q > 1.3$ disk, where the swing amplification is very weak. This proves that the swing amplification is the reason for the formation of the transient spiral structures seen in the central regions of the $Q \sim 1$ disk.

We additionally performed a simulation with self-gravity of the disk turned off with a $Q \sim 1$ disk in a T_2 halo, whose result is shown in Figure 11. No transient spiral structures form in this simulation, although two-armed grand-design spiral structures still form. Without self-gravity, there is no swing amplification process in the disk. This further demonstrates that transient arms are caused by the swing amplification, while two-armed grand-design spiral structures are not formed due to the swing amplification.

We also compare the simulations with $Q \sim 1$ disks in S and T_2 haloes as shown in Figure 10. Transient spiral struc-

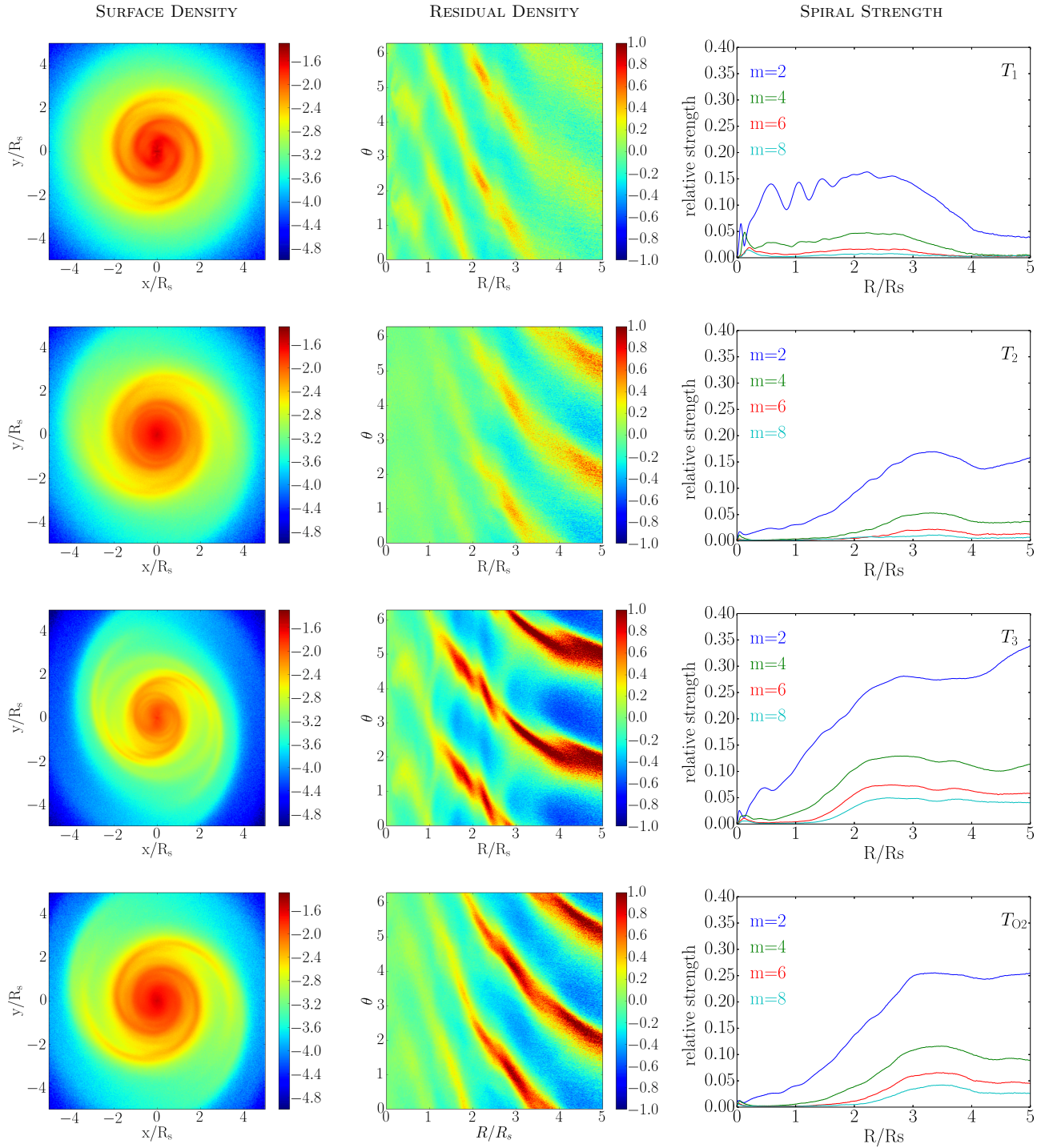


Figure 8. Surface density, residual density and spiral structure strength of disks in simulations with T_1 , T_2 , T_3 and T_{O2} haloes (from top to bottom). Left column: surface density in Cartesian coordinates at time $t = 0.5$ Gyr. Central column: residual density in polar coordinates at time $t = 0.5$ Gyr. Right column: spiral strength for different modes averaged over a time interval from 0.35 Gyr to 0.85 Gyr. This time interval is chosen so that the spiral structures are fully developed in the disk. Note that spiral strengths with the odd m modes are not shown because they are much weaker. For the halo that is more triaxial inside (T_1), the spiral structure is stronger inside, while for the halo that is more triaxial outside (T_2), the spiral structure is also stronger outside. For T_3 halo which has $b/a \sim c/a \sim 0.85$, the spiral structure strength is generally higher than the other two simulations, except for the central region where the spiral structures strength is lower than that of the T_1 halo. For the T_{O2} halo, the disk plane is determined by the direction of the total angular momentum, as discussed later in Section 3.5.

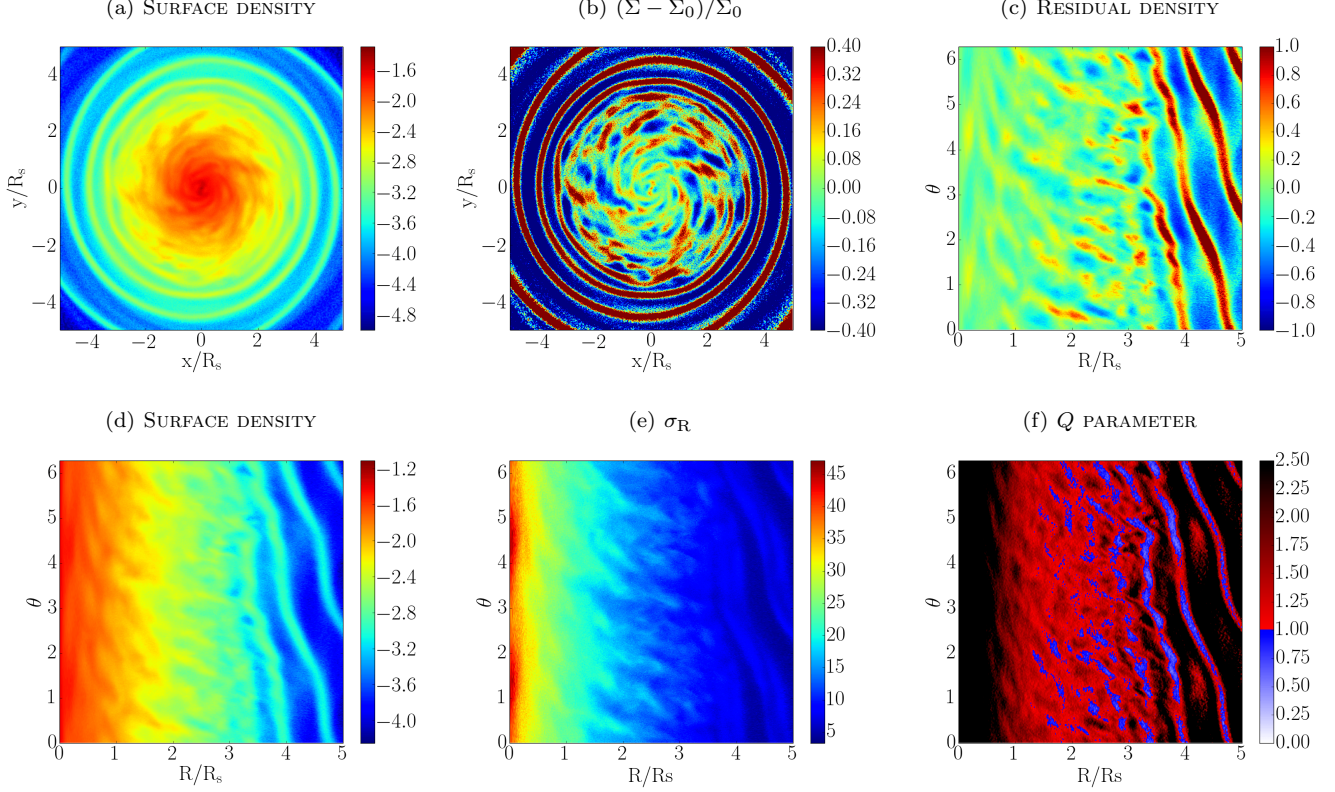


Figure 9. Maps of various quantities of a $Q \sim 1$ stellar disk in the T_2 halo at time 3 Gyr. (a) shows the surface density in Cartesian coordinates. To show the structures throughout the disk more clearly, we subtracted the initial surface density Σ_0 from the surface density Σ at 3 Gyr and then divided it by Σ_0 . The result is shown in (b). (c) shows the residual density map in polar coordinates. In (d), (e) and (f), surface density, dispersion of the velocity in radial direction, σ_R , and Q parameter are shown in polar coordinates. Two different types of spiral structures co-exist in the disk. Outside $3.5R_S$ is the grand design two-folded spiral structure caused by the triaxial halo, while inside $3.5R_S$ there are more arms and they are all transient.

tures form in both cases. However, the transient spiral structures formed in the T_2 halo are significantly stronger than that formed in the S halo. For the simulation with the T_2 halo, two-armed spiral structures formed in the central region of the disk at early times are gradually swing amplified and form the first generation of transient spiral structures later, while for the simulation with the S halo, transient spiral structures form due to the swing amplification of the Poisson noise in the initial conditions. With 10^8 particles in the disk, the Poisson noise is much weaker perturbation to the density field of the disk than grand-design spiral structures. Therefore transient spiral structures formed in a T_2 halo are much stronger than that in a S halo.

To understand the formation mechanism of two-armed spiral structures, we measured the power spectra of the disks in T_2 haloes. The surface density Σ of the disk at time t , radius R and azimuthal angle θ can be expressed by the summation of a series of waves

$$\Sigma(R, \theta, t) = \sum_{\Omega_f} \sum_m A(R, m, \Omega_f) e^{i(\Omega_f t + m\theta)}, \quad (18)$$

where m is the number of arms and $\Omega_f = m\Omega_p$ is m times the pattern speed Ω_p . Values of $A(R, m, \Omega_f)$ are complex numbers. We are more interested in the absolute value $|A(R, m, \Omega_f)|$, which is the strength of the wave. The power spectra are a good tool to study the waves in the disk. In our

simulations, since the surface density in the central region is much higher than that in the outer region, small fluctuations in the centre can have a higher power than the spiral structures located further out. In order to show the power spectra of the spirals clearly, we calculate power spectra of the residual surface density instead of the surface density.

Power spectra of $Q \sim 1$ and $Q > 1.3$ disks in T_2 haloes for a time interval from 2 Gyr to 7.5 Gyr are shown in Figure 12. For the power spectra of $m = 2$ modes, the highest power lies at the inner Lindblad resonance where the pattern speed is $\Omega_P = \Omega - \kappa/2$, with Ω being the rotation speed of the stars and κ being the epicyclic frequency. The high power region in the power spectra of the $m = 2$ modes of the $Q > 1.3$ disk spans throughout the disk, but the high power region for the $Q \sim 1$ disk is located only at the outer region of the disk. This is because the inner region of the $Q \sim 1$ disk is disrupted by the swing amplification, as previously shown in Figure 10. For the power spectra of $m = 9$ modes, the power strength of the $Q \sim 1$ disk is more than 5 times higher than that of the $Q > 1.3$ disk, because the latter does not form prominent transient multi-armed spiral structures. Horizontal structures present in the power spectra for the $m = 9$ modes of the $Q \sim 1$ disk, are shown to be the characteristic features of the transient spiral structures due to the swing amplification by Sellwood & Carlberg (2014).

The fact that the regions of the highest power of $m = 2$

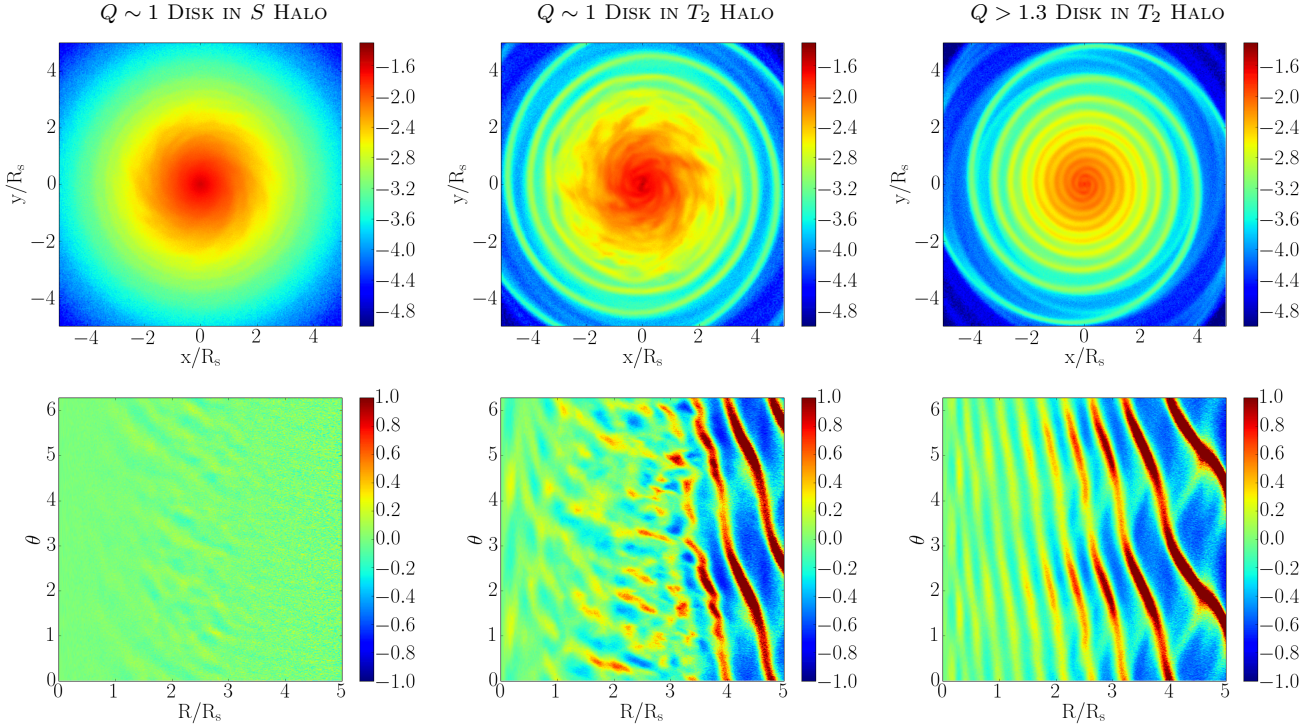


Figure 10. Surface density (top row) and residual density (bottom row) for disks in three different simulations at time $t = 3$ Gyr. By comparing the left and the middle column we find that the strength of the transient spiral structures is stronger for the disk in a triaxial halo, although they are both formed due to swing amplification. As shown in the right column, transient multi-armed spiral structures do not form with a more stable ($Q > 1.3$) disk.

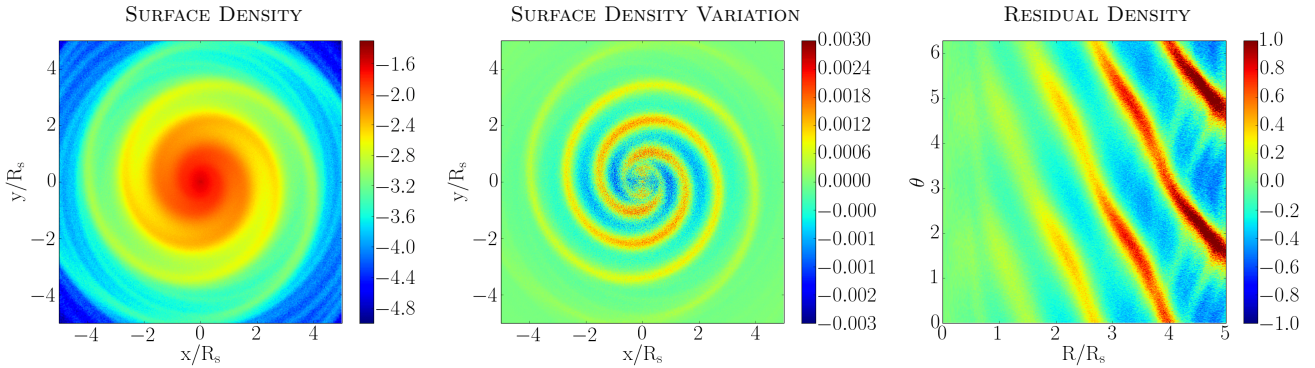


Figure 11. Simulation of $Q \sim 1$ disk in T_2 halo without self-gravity at time $t = 3$ Gyr. Without self-gravity, transient spiral structures no longer form, while the grand-design spiral structures still persist.

modes lie at the inner Lindblad resonance indicates that the two-armed grand-design spiral structures are indeed kinematic density waves, as proposed by Lindblad (1956). For a large region in the disk, the value of $\Omega - \kappa/2$ in our simulations can be regarded as roughly constant. Due to the epicyclic motion of the stars, in a frame rotating with this angular speed, stars have stationary elliptical orbits. Therefore in such a frame if the orbits of the stars are arranged to be more crowded in some regions than the others initially, the crowded regions will remain crowded. Seen from a rest frame, this corresponds to a pattern moving with the pattern speed $\Omega_P = \Omega - \kappa/2$. In our simulations, such arrangement of the orbits is caused by sudden introduction of triaxial haloes. Once formed, such patterns can survive in

the disk for several Gyrs (see also Figure 6 and discussion in Section 3.2).

The life-times of grand-design spirals are shown in Figure 13. Here we plot the strength of the $m = 2$ modes as a function of time for radii $R = 1R_S, 3R_S$ and $5R_S$. For simulations with $Q > 1.3$ disks, in general, spiral strengths peak at $1 \sim 4$ Gyr and then gradually decline. Spiral strengths larger than 0.1 can persist for up to 5 – 10 Gyrs, depending on the radius probed. The peak values correlate strongly with the torque strength shown in Figure 7, i.e. the peak value of the spiral strength is stronger when the torque strength is stronger. For the simulation with a $Q \sim 1$ disk and a T_2 halo, at the beginning, the growth of the spiral strength is similar to the simulation with the same halo but with a $Q > 1.3$

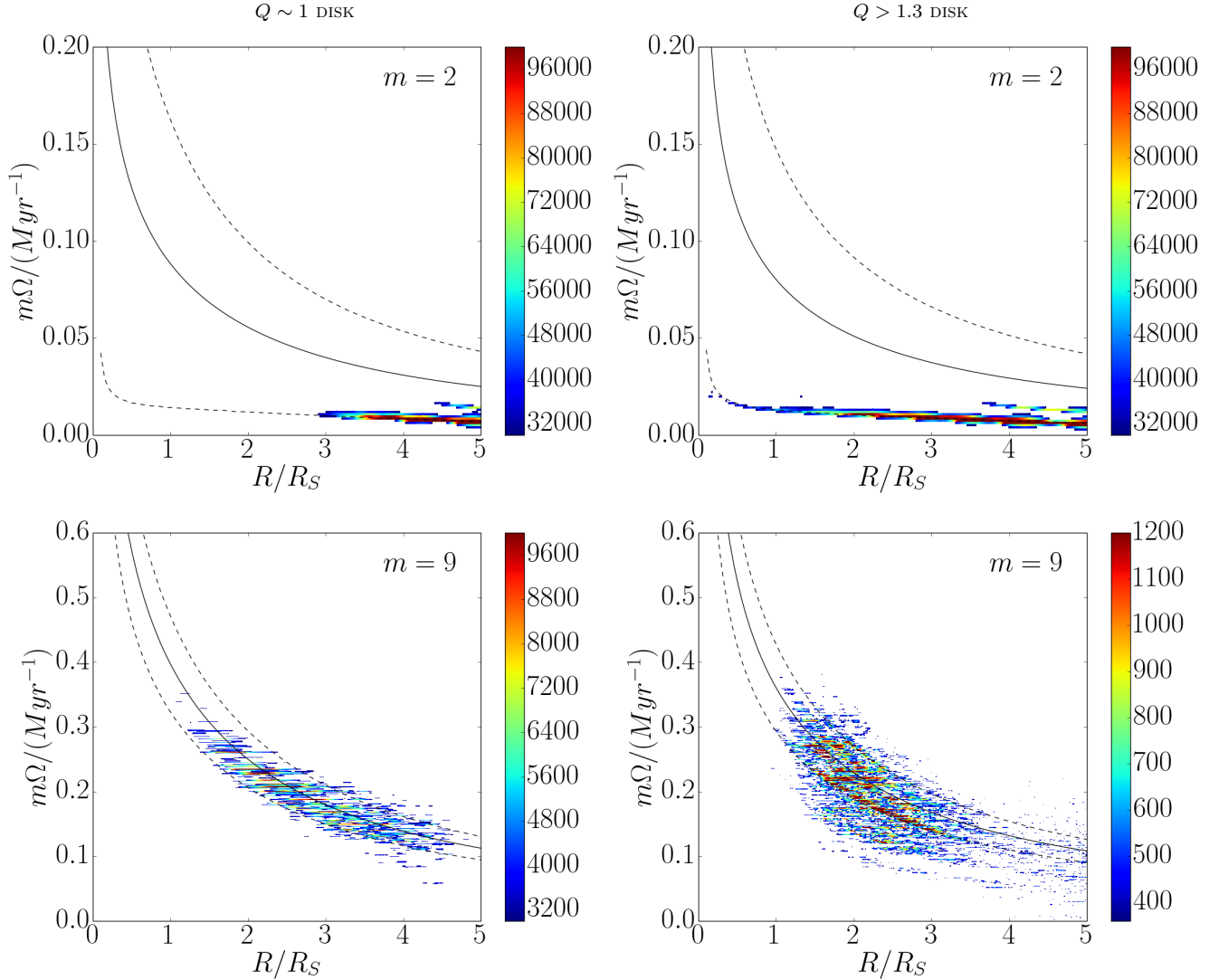


Figure 12. Power spectra of the $Q \sim 1$ disk (left) and the $Q > 1.3$ disk (right) for a time interval 2 Gyr to 7.5 Gyr in T_2 haloes for $m = 2$ modes (top) and $m = 9$ modes (bottom). On each panel black solid curve indicates corotation line with pattern speed $\Omega_P = \Omega$, where Ω is the angular velocity of the stars, while black dashed curves are inner and outer Lindblad resonances with $\Omega_P = \Omega \pm \kappa/2$, with κ being the epicyclic frequency. For $m = 2$, the dominating feature corresponds to the grand-design spiral structures. For the $Q \sim 1$ disk this structure only exists in the outer region, because the grand-design spiral structures are distorted by swing amplification. For the $Q > 1.3$ disk where swing amplification is weak, the grand-design spiral modes extend down to the innermost regions. The grand-design spiral structures lie at the inner Lindblad resonance. The dominating features of $m = 9$ modes are the horizontal structures crossing the co-rotation line, which are the typical structures of swing amplified modes. The strength of these modes in $Q > 1.3$ disk is roughly an order of magnitude lower than in the $Q \sim 1$ disk, as can be seen from the colour bar. Other high- m modes are not shown, as they are all qualitatively similar to the $m = 9$ power spectra.

disk, but the strength of the spirals in the $Q \sim 1$ disk starts to decrease earlier, in 1 to 2 Gyr. This is the time when the $Q \sim 1$ disk starts to develop transient spiral structures due to swing amplification, which favours spiral structures with higher m modes.

3.5 Disks in Misaligned Triaxial Haloes

We now focus onto the influence of triaxial haloes if the disk does not lie in the $x - y$ plane of the halo. The top row of Figure 14 shows the projection of the disk onto its initial plane in the simulation with a T_{O2} halo, i.e. a halo that is more triaxial outside with the disk plane that initially has a

45° angle with respect to the $x - y$ plane of the halo, at three different times, $t = 0.7$ Gyr, 1.3 Gyr and 2 Gyr. At 0.7 Gyr, the overall shape of the projection starts to be compressed. This compression becomes stronger over time. At around $t = 2$ Gyr, the projection of the disk is strongly compressed in one direction. This compression of the projection onto a fixed plane indicates that the inclination of the disk in changing. In a triaxial halo, the gravity force does not always point directly to the centre. It does not even lie in the disk plane if the disk plane does not coincide with $x - y$, $x - z$ or $y - z$ plane of the halo. The perpendicular component of the gravity force results in a non-zero torque that is not in the

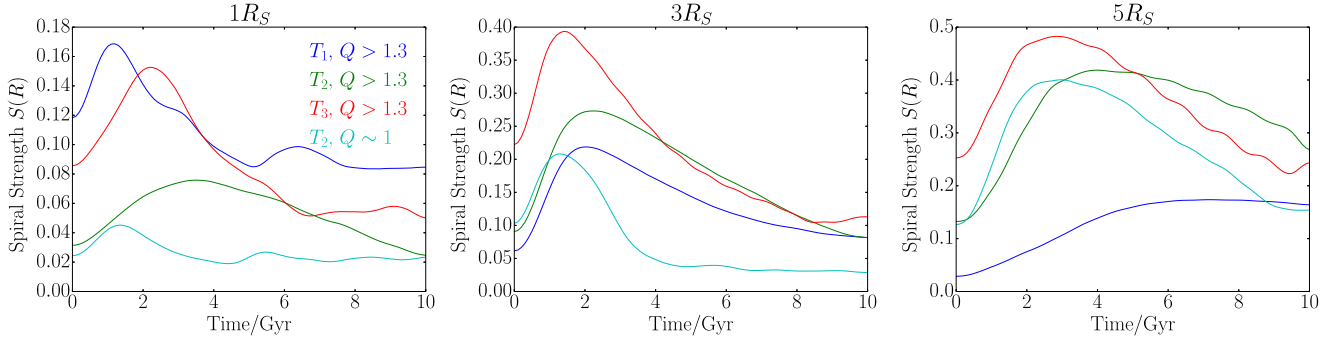


Figure 13. The strength of the $m = 2$ spiral structures as a function of time for radii $R = 1R_S, 3R_S$ and $5R_S$ in various simulations. Curves have been smoothed over a ~ 2 Gyr time-span to show the general trends more clearly. For simulations with $Q > 1.3$ disks, spiral strengths peak at 1 to 4 Gyr and then gradually decrease over several Gyrs. In the T_2 halo with $Q \sim 1$ disk the strength of grand-design spirals is affected by transient spirals after 1 – 2 Gyrs.

direction of angular momentum, which leads to the change of the disk’s inclination.

We can infer the normal direction of the disk with the direction of the angular momentum vector, as long as the stars stay roughly in a plane. To achieve this we calculate the total angular momentum

$$L = \sum_i m \mathbf{r}_i \times \mathbf{v}_i \quad (19)$$

at each timestep, where m is the mass of a single particle, \mathbf{r}_i and \mathbf{v}_i are the position and velocity vector of the i -th star particle.

The middle row of Figure 14 shows the projection of the disk onto the plane that is perpendicular to the total angular momentum vector. We can see that the morphology of the spiral structures is similar to the disk that is not misaligned with respect to the $x - y$ plane of the halo, for example similar to the disk shown in Figure 9. However, in the outer parts of the disk the shape of the spiral arms is distorted.

We can understand the distortion of the disk by looking at it edge-on. As shown in the bottom row of Figure 14, the disk develops a integral shape warp at later times, indicating that the disk no longer stays in a plane. Also more and more mass spreads along the z -direction. It is also worth noticing that though the warping of the disk shows a trend for the disk to become aligned with the major axis of the halo, which is 45° from the initial normal direction of the disk, in fact most of the mass of the disk stays in roughly the same initial plane at time $t = 2$ Gyr.

The warp of the disk before 0.75 Gyr is very weak. Therefore we can compare the strength of the spiral structures at early times, e.g. 0.5 Gyr, in this simulation with the simulations where the disks lie in the $x - y$ plane of the triaxial halo, as shown in the bottom row of Figure 8 and the right panel of Figure 7. The strength of the spiral structures in this simulation also matches with the gravitational torque caused by the triaxial halo. In fact, the strength of the torque in this simulation lies between the simulations with T_2 and T_3 haloes, as well as the corresponding strength of the spiral structures.

At later times, the outer part of the disk no longer stays in the disk plane. As shown in the middle row of Figure 14, the outer part of the spiral structures is distorted. We plot the density projection of the disk in polar coordinates, as

illustrated in the left panel of Figure 15. For $R/R_S > 3.5$, radius of the spiral structures no longer increases strictly as the angle goes counter-clockwise. To investigate if this is due to the warp of the disk, we rotate every pixel in this plot onto the disk plane again while keeping the azimuthal coordinate θ unchanged, so that the spiral structure all through the disk can be compared on the same plane. This is done by changing the radius R of each pixel to $\sqrt{R^2 + \bar{z}^2}$, where

$$\bar{z} = \frac{1}{\Sigma(R, \theta)} \int_{-\infty}^{\infty} \rho(R, \theta, z) z dz, \quad (20)$$

is the mean height of the mass at (R, θ) . The result is shown in the right panel of Figure 15. The radius of the spiral structures increases strictly counter-clockwise, as is the case for the spiral structures in all other simulations with disks in the $x - y$ plane of the halo. This indicates that the distortion of the outer part of the spiral structures is simply due to the projection.

In conclusion, when the disk is misaligned with the halo, the spiral structures still grow in response to the torque. Their strength corresponds to the strength of the torque, similar to the simulations with disks lying in the halo plane. Even though warps develop at later times, they interfere very little with the spiral structures. The morphology of the spiral structures are unaffected as long as the radius of the spiral structures are calculated with the height from the disk taken into account.

4 CONCLUSIONS

In this paper we used very high resolution N-body simulations to investigate the influence of triaxial haloes onto stellar disks, especially on the formation of spiral structures. In our simulations the haloes are implemented as analytic potentials rather than dark matter particles to minimize possible numerical artifacts caused by Poisson noise and to allow to perform many very high resolution simulations of the stellar disks, which are represented with up to 10^8 particles. While disks with $Q > 1.3$ are stable against spiral structures in spherical haloes, we found that two-armed grand-design spiral structures form in such disks if they are embedded within triaxial haloes. These spiral structures extend all the way to the edge of the disk. Their strength dependence with

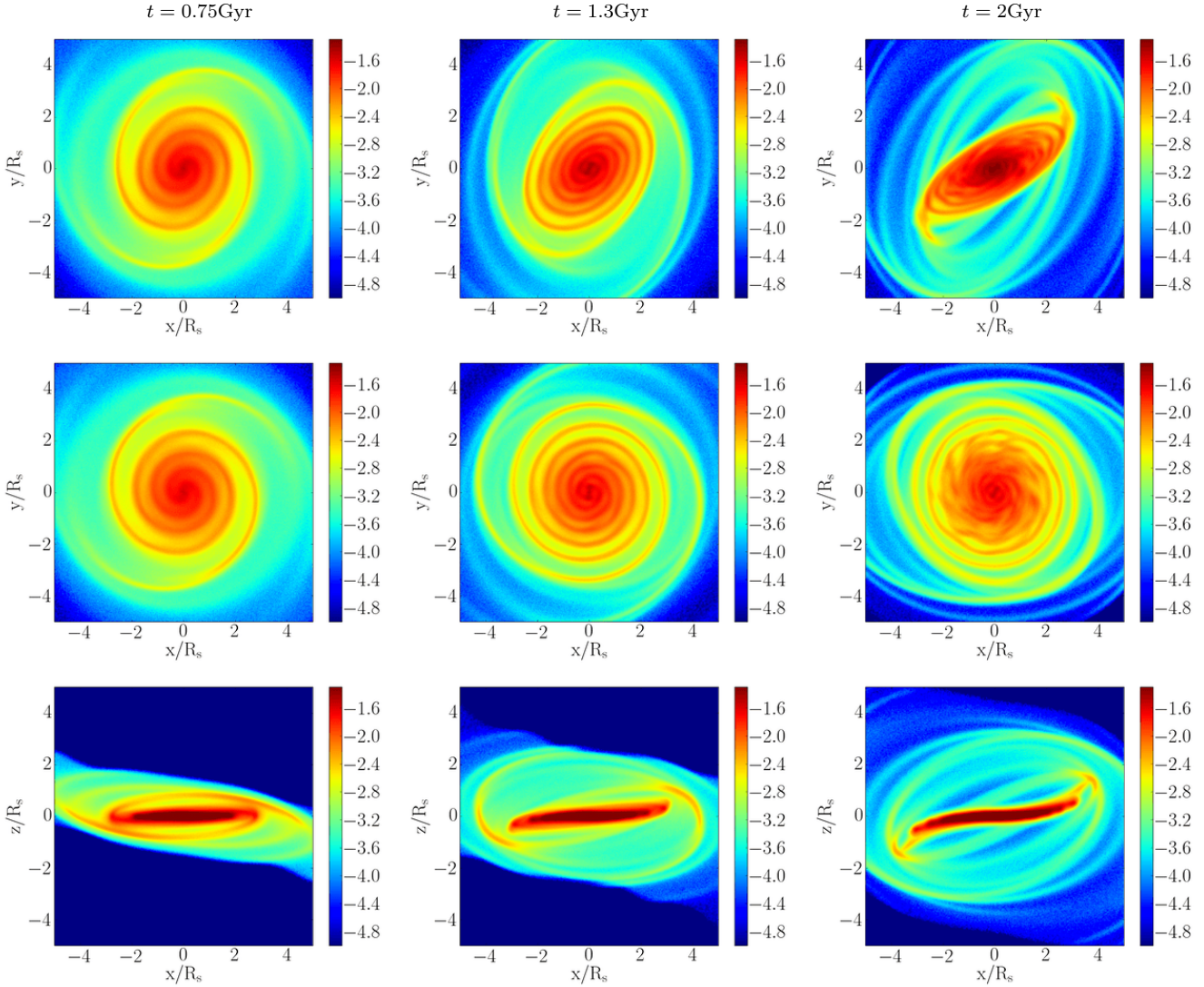


Figure 14. Evolution of a disk in a misaligned triaxial halo. Top: projection of density on the initial plane. Middle: projection of density on the disk plane, whose normal direction is defined by the total angular momentum. Bottom: edge-on column density of the disk. Grand-design two-armed spiral structures still form in this case, while the orientation of the disk is changing as well. It can be also seen from the edge-on plot that warps develop in the disk at later times.

radius is determined by the torque from the triaxial halo experienced by the disk. We further showed that these spiral structures have the following features:

- They do not form when the halo turns from spherical to triaxial adiabatically. This indicates that the impulsive introduction of triaxial haloes leads to the grand-design two-armed spiral structures.
- They form in disks that have $Q > 1.3$, i.e. when the swing amplification process is weak in the disk. This demonstrates that swing amplification is not necessary for the formation for these spiral structures.
- They form even if the self-gravity of the disk is turned off, which again excludes swing amplification as the essential formation mechanism.
- Once formed, they can survive in spherical haloes. Triaxial haloes are therefore not necessary for maintaining the spiral structure.
- Their power spectra peak at the inner Lindblad reso-

nance that satisfies $\Omega_P = \Omega - \kappa/2$, which is almost flat for a large region of the disk in our model, in agreement with the kinematic density wave theory proposed by Lindblad (1956).

Furthermore, we showed that the swing amplification process and the impulsive change of the halo triaxiality can in fact interfere with each other. When the time scale of the growth of transient spiral structures due to the swing amplification is very short, which in our case occurs when the number of the star particles used in the simulation is low, only transient arms form, while their distribution becomes more asymmetric in a triaxial halo. When the process of swing amplification is slow enough, two-armed grand-design spiral structures form in the first place. However these spiral structures break up and get swing amplified into transient arms at later times. Moreover, at a given resolution spiral structures formed in this way grow faster than those formed in a spherical halo where the Poisson noise in the initial conditions is the only source for the swing amplification.

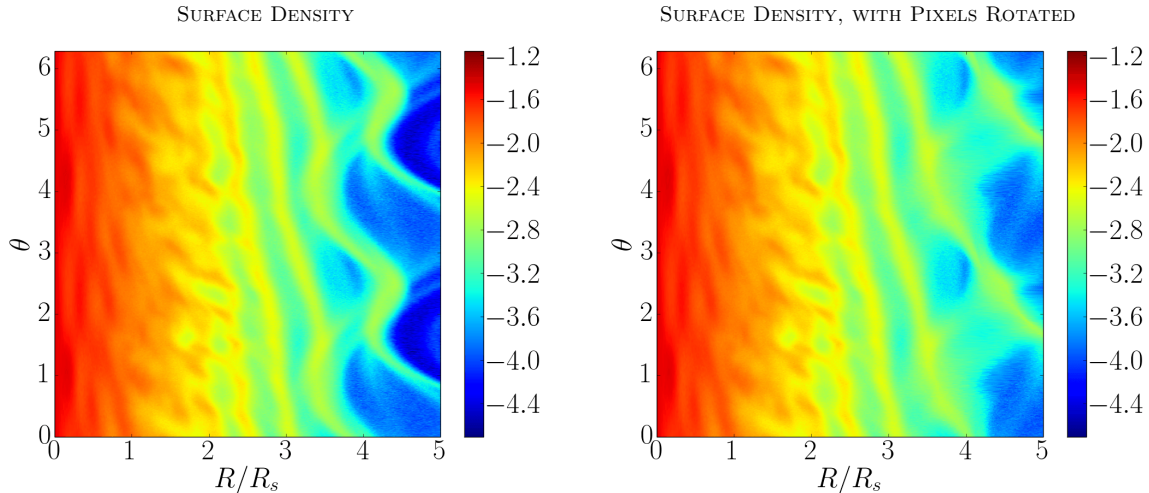


Figure 15. Surface density of a disk in a misaligned triaxial halo at 2Gyr in polar coordinates. The outer part of the disk is not in the plane defined by the angular momentum of the disk. The spiral arms are distorted if the density is directly projected onto the disk plane (left). However, if we rotate every pixel onto the disk plane (right), the morphology of the spiral structure becomes similar to the simulations with disks within the $x - y$ plane of the haloes.

When the disk is misaligned with the major axes of the halo, it no longer stays in a plane as it evolves. Integral shaped warps form in the disk. Two-armed spiral structures still form and are similar to those formed in disks that lie in the $x - y$ plane of the triaxial haloes. However, the outer parts of the spiral structure are distorted, due to the fact that they are no longer in the disk plane.

The sudden introduction of triaxiality into an initially spherical halo in equilibrium with the stellar disk is clearly a very idealized setup and is not directly applicable to observed systems. However we have shown that similar spiral structures develop as long as the time scale of the gravitational potential perturbation is shorter than the orbital period of stars. Massive satellite flybys, mergers and tumbling triaxial haloes are known to alter gravitational potentials rapidly and to introduce torques. The formation of spiral structures in these cases likely shares a similar underlying mechanism with our simulations, where the strength of arms formed depends on the gravitational torques, and where grand-design arms form. Furthermore, if stellar disks are subject to swing amplification, additional rapid perturbations in gravitational potentials and torques might be conducive to the development of transient arms.

ACKNOWLEDGEMENTS

We thank Cathie Clarke, Christophe Pichone, Jim Pringle and Giuseppe Lodato for their useful comments and advice. SH is supported by the CSC Cambridge Scholarship, jointly funded by the China Scholarship Council and by the Cambridge Overseas Trust. This work was performed on: DiRAC Darwin Supercomputer hosted by the University of Cambridge High Performance Computing Service (<http://www.hpc.cam.ac.uk/>), provided by Dell Inc. using Strategic Research Infrastructure Funding from the Higher Education Funding Council for England and funding from the Science and Technology Facilities Council; DiRAC Complexity system, operated by the University of Leicester IT

Services, which forms part of the STFC DiRAC HPC Facility (www.dirac.ac.uk). This equipment is funded by BIS National E-Infrastructure capital grant ST/K000373/1 and STFC DiRAC Operations grant ST/K0003259/1. DiRAC is part of the National E-Infrastructure.

REFERENCES

- Arp H., 1966, *The Astrophysical Journal Supplement Series*, 14, 1
- Barnes J., Efstathiou G., 1987, *The Astrophysical Journal*, 319, 575
- Bertin G., Lin C. C., 1996, *Spiral structure in galaxies a density wave theory*. Cambridge, MA MIT Press
- Binney J., 1987, *Galactic dynamics*. Princeton university press
- Bowden A., Evans N., Belokurov V., 2013, *Monthly Notices of the Royal Astronomical Society*, 435, 928
- Bryan S. E., Kay S. T., Duffy A. R., Schaye J., Dalla Vecchia C., Booth C. M., 2013, *MNRAS*, 429, 3316
- Churchwell E., Babler B. L., Meade M. R., Whitney B. A., Benjamin R., Indebetouw R., Cyganowski C., Robitaille T. P., Povich M., Watson C., et al., 2009, *Publications of the Astronomical Society of the Pacific*, 121, 213
- DeBuhr J., Ma C.-P., White S. D., 2012, *Monthly Notices of the Royal Astronomical Society*, 426, 983
- Dobbs C., Baba J., 2014, *PASA*, 31, 35
- Dobbs C. L., Bonnell I. A., 2006, *MNRAS*, 367, 873
- Dobbs C. L., Bonnell I. A., 2007, *MNRAS*, 376, 1747
- D’Onghia E., Springel V., Hernquist L., Keres D., 2010, *ApJ*, 709, 1138
- D’Onghia E., Vogelsberger M., Hernquist L., 2013, *The Astrophysical Journal*, 766, 34
- Dubinski J., 1994, *ApJ*, 431, 617
- Dubinski J., Chakrabarty D., 2009, *The Astrophysical Journal*, 703, 2068
- Fouvry J.-B., Pichon C., 2015, *MNRAS*, 449, 1982

- Frenk C. S., White S. D., Davis M., Efstathiou G., 1988, *The Astrophysical Journal*, 327, 507
- Fujii M. S., Baba J., Saitoh T. R., Makino J., Kokubo E., Wada K., 2011, *ApJ*, 730, 109
- Gittins D. M., Clarke C., 2004, *Monthly Notices of the Royal Astronomical Society*, 349, 909
- Goldreich P., Lynden-Bell D., 1965, *Monthly Notices of the Royal Astronomical Society*, 130, 125
- Hernquist L., 1990, *The Astrophysical Journal*, 356, 359
- Jing Y., Mo H., Börner G., Fang L., 1995, *Monthly Notices of the Royal Astronomical Society*, 276, 417
- Jing Y., Suto Y., 2002, *The Astrophysical Journal*, 574, 538
- Kalnajs A., 1973, in *Proceedings of the Astronomical Society of Australia Vol. 2, Spiral structure viewed as a density wave*. p. 174
- Khoperskov A. V., Khoperskov S. A., Zasov A. V., Bizyaev D. V., Khrapov S. S., 2013, *MNRAS*, 431, 1230
- Khoperskov S. A., Bertin G., 2015, *MNRAS* accepted, arXiv:1505.04598
- Lin C., Shu F. H., 1964, *The Astrophysical Journal*, 140, 646
- Lindblad B., 1956, *Stockholms Observatoriums Annaler*, 19, 7
- Lindblad B., 1963, *Stockholms Observatoriums Annaler*, 22, 5
- Miller R., 1972, in *Gravitational N-Body Problem*. Springer, pp 213–230
- Sellwood J. A., 2012, *ApJ*, 751, 44
- Sellwood J. A., Carlberg R. G., 2014, *ApJ*, 785, 137
- Springel V., 2005, *Monthly Notices of the Royal Astronomical Society*, 364, 1105
- Springel V., Di Matteo T., Hernquist L., 2005, *Monthly Notices of the Royal Astronomical Society*, 361, 776
- Thomas P. A., Colberg J. M., Couchman H. M., Efstathiou G. P., Frenk C. S., Jenkins A. R., Nelson A. H., Hutchings R. M., Peacock J. A., Pearce F. R., et al., 1998, *Monthly Notices of the Royal Astronomical Society*, 296, 1061
- Toomre 1964, *The Astrophysical Journal*, 139, 1217
- Toomre 1981, in *Structure and evolution of normal Galaxies Vol. 1, What amplifies the spirals*. pp 111–136
- Warren M. S., Quinn P. J., Salmon J. K., Zurek W. H., 1992, *The Astrophysical Journal*, 399, 405
- Yoshida N., Springel V., White S. D., Tormen G., 2000, *The Astrophysical Journal Letters*, 544, L87
- Zemp M., Gnedin O. Y., Gnedin N. Y., Kravtsov A. V., 2012, *The Astrophysical Journal*, 748, 54
- Zhu Q., Marinacci F., Maji M., Li Y., Springel V., Hernquist L., 2015, *MNRAS* submitted, arXiv:1506.05537

APPENDIX A: DISK STABILITY IN SPHERICAL HALO

Fujii et al. (2011), Sellwood (2012), D’Onghia et al. (2013) and several other works have found that the Poisson noise in the disk due to a low number of star particles can be greatly swing amplified causing transient spiral structures to form. As stated in Section 3.1, we performed several simulations to study this effect. These simulations include one simulation with a $Q > 1.3$ disk containing 10^8 star particles and four simulations with $Q \sim 1$ disks containing 10^5 , 10^6 , 10^7

and 10^8 star particles. Surface density of disks at 2.5 Gyr are shown in Figure A1. Strong spiral structures form in simulation with 10^6 and 10^7 star particles, while very weak spiral structures are present in simulation with 10^8 star particles. For the simulation with 10^5 star particles, the spiral structures can barely be seen due to two reasons: a) as shown in Figure 1, the strength of spiral structures in this simulation decreases after several hundred million years, b) number of particles is too low to show weak spiral structures.

For simulations with 10^6 to 10^8 star particles, the spiral structures are most prominent in the region $R_S < r < 3R_S$. We checked the evolution of such spiral arms and found that each single arm is not long-lived. The arms break up quickly and new arms emerge from the fragments of the old arms. The stars in the disk are rotating counter-clockwise, therefore the spiral structures are trailing, which is in the agreement with the prediction of the swing amplification mechanism.

The average Q value as a function of radius is shown in Figure A2. Blue lines denote the Q value in the initial conditions. Q parameter for simulations with $Q \sim 1$ disks are shown with solid curves. While for the majority of disks Q is set to be no less than 1 initially, for $R_S < r < 2R_S$, the Q parameter is close to or slightly lower than 1. Swing amplification is most efficient when Q is slightly over 1, which corresponds to the range of radii of $2R_S < r < 3R_S$. Therefore in the region of $R_S < r < 3R_S$, the Q parameter is either less than 1 or slightly over 1. This explains why transient spiral structures are strongest in this region. For simulation with low number of particles, Q value grows over time. At later times, Q is so high that swing amplification is no longer strong, which leads to the decreasing of spiral strength. In the simulation with a disk with $Q > 1.3$, Q parameter is higher than 1.3 all through the disk, as shown in the bottom right panel of Figure A2 with dashed curves. Due to a high Q , spiral structures do not grow in the $Q > 1.3$ disk.

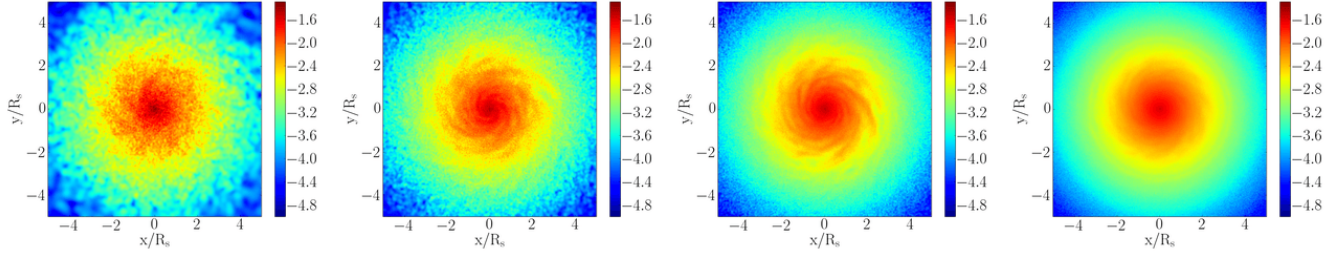


Figure A1. Surface density of the stellar disk with $Q \sim 1$ at time $t = 2.5\text{Gyr}$. Four simulations with increasing number of particles, ranging from 10^5 (left) to 10^8 (right), are shown. Strong spiral structures develop when the particle number is lower than 10^8 , while for the disk with 10^8 particles, very weak spiral structures can also be seen. For 10^5 particles, the spiral structures initially present fade away before $t = 2.5\text{Gyr}$.

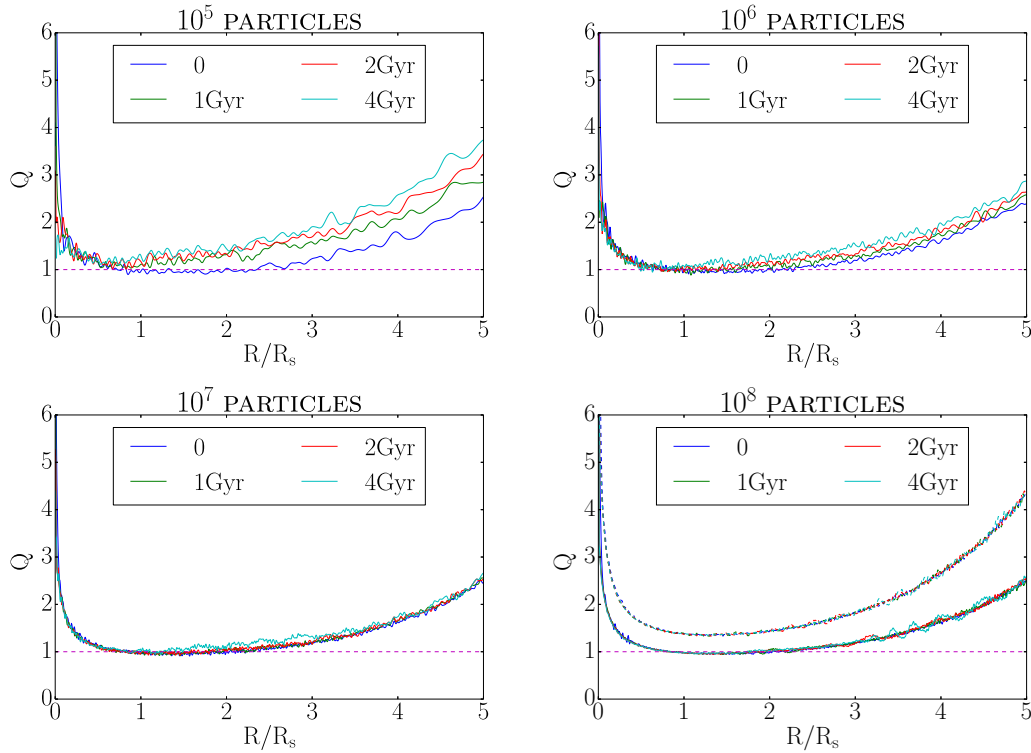


Figure A2. Toomre's Q parameter as a function of radius. Plots for four identical $Q \sim 1$ disks simulated with different number of particles (from 10^5 to 10^8) are shown with solid lines, while a $Q > 1.3$ disk is shown with dashed lines in the bottom right panel. Lines of different colour stand for different times, as annotated in legends. In particular, blue lines in each plot denote the $Q - r$ relation at the initial time. The disk is unstable to swing amplification if Q is close to 1. As spiral structures develop, the “temperature” of the disk raises for low particle numbers, i.e. 10^5 and 10^6 , resulting in an increase of Q at later times. This increase of Q coincides with the decrease of spiral strength of corresponding models shown in Figure 1.